

ST7 DISTURBANCE REDUCTION SYSTEM (DRS) COLLOID MICRONEWTON THRUSTER

PERFORMANCE AND CONTROL ALGORITHM MODEL SIMULATION

VALIDATION IN FLIGHT

Colleen Marrese-Reading, John Ziemer, Curt Cutler, Charley Dunn, Andrew Romero-Wolf,
Shahram Javidnia, Thanh Le, Irena Li, Phil Barela
Jet Propulsion Laboratory, California Institute of Technology
Pasadena, CA

Jacob Slutsky, James Ira Thorpe, Peiman Maghami, Oscar Hsu, James O'Donnell,
NASA Goddard Space Flight Center
Greenbelt MD, 20771

Nathaniel Demmons and Vlad Hruby
Busek Co.
Natick, MA 01760

ABSTRACT

Colloid Micronewton Thrusters (CMNT) were flight demonstrated for the first time on the ST7-Disturbance Reduction System (DRS) payload on the European Space Agency (ESA) Laser Interferometer Space Antenna (LISA) Pathfinder spacecraft for attitude and drag-free spacecraft control. LISA Pathfinder was a technology demonstration mission for ESA's LISA gravitational wave observatory, currently in Phase A with a launch date of 2034. The DRS included the Integrated Avionics Unit (IAU), eight Colloid Micronewton Thrusters (CMNT), Dynamic Control Software (DCS) and Flight Software (FSW). The CMNT technology met performance requirements operating at 5-30 μN of thrust with $\leq 0.1 \mu\text{N}$ resolution and $\leq 0.1 \mu\text{N}/\sqrt{\text{Hz}}$ thrust noise to deliver the required nanometer-level precision spacecraft control measured by the gravitational reference sensor (GRS) in the ESA LISA Technology Package (LTP). The performance of seven of the CMNT in flight was consistent with ground test results. The colloid thruster performance model of thrust and thrust noise as a function of operational parameters (i.e. beam current, voltage, temperature, etc.) was validated in flight over a wide range of conditions. A model and simulation of the thruster control algorithm was developed and validated with flight data to predict thrust noise. This capability is important because it is considered to be a significant source of position noise on the spacecraft and, therefore, the acceleration noise on the test masses, which provide the gravity wave measurements. The CMNT thruster model data and validation with LISA Pathfinder/ST7-DRS flight experiments are discussed in this paper.

INTRODUCTION

The development of a space-based gravitational wave observatory by ESA and NASA required flight validation of the technologies for the gravity wave measurement. An important part of the LISA Pathfinder technology demonstration mission was showing that drag free control could be employed to place a test mass in near-perfect free fall using colloid micronewton thrusters to position the spacecraft to follow the test mass without significantly adding to the acceleration noise. The Laser Interferometer Space Antenna (LISA) mission is under development to launch in 2034 to detect and characterize gravity waves in the milliHertz band with three drag-free spacecraft configured as an equilateral triangle with ~ 2.5 million kilometer arms to detect space-time strains

caused by passing gravity waves. The LISA Pathfinder (LPF) mission was developed and flown by ESA with a NASA payload to demonstrate the concept and capabilities required for this observatory. LPF included the ESA LISA Test Package (LTP) and the NASA ST7-DRS payload, which each employed their own drag-free control algorithms and micropropulsion systems for spacecraft attitude, position and drag-free control. The ST7-DRS payload included the Colloid Micro-Newton Thruster (CMNT) electrospray thruster technology and the LTP used precision cold gas thrusters. LPF is the first mission to flight demonstrate electrospray thrusters for spacecraft control. While they had been under development for tens of years, they were significantly matured for this mission because of unique attributes including significant mass, volume, specific impulse and thrust precision, controllability, and thrust noise advantages for the LISA mission and many other missions. The LPF mission not only demonstrated this technology, it also provided a unique opportunity to characterize the thrust and thrust noise through a range of thrust levels, temperatures and beam voltages and currents using the LPF GRS for each of the 8 thrusters. This validated performance and control algorithm models more extensively and with greater precision than was possible during ground testing because it had picometer resolution interferometry. This introduction section summarizes the mission, the spacecraft, the DRS payload, and the CMNT as discussed elsewhere [1,2,3]. The other sections of the paper discuss the CMNT performance and control algorithm simulation models, the validation approach and the results.

LISA PATHFINDER MISSION

LISA Pathfinder was a recent ESA mission with both ESA and NASA payloads to validate key elements of the measurement concept for the LISA gravitational wave observatory. It was launched from Kourou, French Guiana on December 3, 2015 and arrived at Earth-Sun L1 on January 22, 2016. ST7-DRS went through IAU, FSW and all thruster commissioning in January 2016 with the propulsion module attached and the test masses held by launch locks. Attitude measurements using gyroscopes were able to verify operational thrust levels on all eight thrusters to within 10% of expected values, leading to the CMNT system as a viable backup to the cold gas thrusters for tip-off and de-spin activities after separation from the propulsion module. The ESA LTP began executing its primary mission on March 1st, 2016. Then full DRS instrument commissioning was conducted in July to August 2016, prime mission and experiment from August to December 2016, and an extended mission and experiment from March to April 2017. The spacecraft was decommissioned by ESA on July 17, 2017.

An exploded view of the LISA Pathfinder spacecraft is shown in Figure 1. LTP was built by a consortium of European national agencies and ESA. LPF spacecraft sub-systems were integrated and tested under control of Airbus Defense and Space GmbH (LTP Architect). The industrial prime contractor was Airbus Defense and Space, Ltd. The spacecraft carries a cold gas propulsion system and a drag-free attitude control system (DFACS). The basic components of the drag-free system are the test mass, which resides inside the spacecraft but makes no contact with it; a metrology system that measures the position and attitude of the test mass relative to the spacecraft; a control system that determines what forces and torques to apply to the spacecraft and possibly the test mass; and an actuation system that can apply forces and torques to the spacecraft and possibly the test mass. The LISA Technology Package (LTP), included two test masses, each with six-degree of freedom electrostatic metrology and control; an optical interferometer that precisely measures the position and attitude of the test masses much more precisely than the electrostatic system, but in a restricted set of degrees-of-freedom; and a system to monitor and control the thermal magnetic and charge environment of the instrument. The test masses are cubes of gold platinum alloy and function as mirrors for the interferometer and references for DFACS. The gravitational reference sensor (GRS) was the two freely floating test masses within a housing and a measurement system for determining the position of the test masses with respect to the housing and to each other. In order to validate the performance of a gravitation sensor, the motion of one of the test masses must be compared to a reference trajectory provided by the other. The time variation of the separation of the two test masses was used to determine whether external forces had been reduced to the required level necessary to enable future gravitational wave measurement missions. The ESA-provided spacecraft included its own

set of drag-free control laws and its own cold-gas micro-propulsion system. LTP's drag-free system was used for the majority of LPF's operations and achieved a level of performance significantly exceeding the LPF requirements (which were relaxed from the LISA requirements) and meeting or exceeding the requirements for LISA [2]. Spacecraft attitude and drag-free control was also demonstrated with the ST7-DRS control algorithms and colloid thrusters. During phases of the LPF mission where ST7-DRS operated, NASA's colloid thrusters were used in place of ESA's cold gas thrusters to move and orient the spacecraft, with the DRS control laws replacing the ESA control laws. An illustration of the DRS concept is in Figure 2. During ST7 operations, the rest of the LTP payload played the same role as during the LTP-led parts of the mission, by providing information on the positions and attitudes of the test masses and applying forces and torques to the test masses, as requested by the DRS controllers. The primary purpose of the ST7-DRS operations were to measure and characterize the performance of these two subsystems, with consideration for their potential use in LISA or other missions. Experiments were conducted with the ST7-DRS to control the spacecraft through different drag-free control modes, observing test mass position and acceleration noise, calibrating the thrusters and validating the performance model and control algorithm model simulations. Eleven significant experiments were conducted during the primary mission and fourteen were conducted during the extended mission. The DRS met all of its mission-level requirements, successfully demonstrating the required performance of the CMNTs and the DCS control laws. [4,5,6,7]

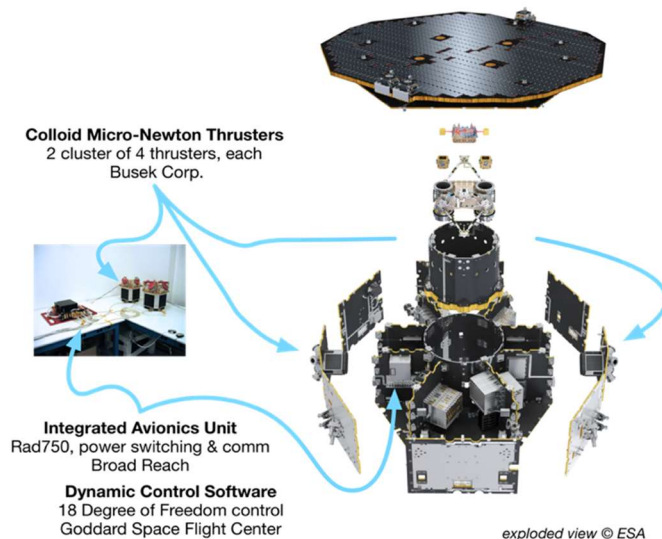


Figure 1. Exploded view of the LISA Pathfinder spacecraft with the ST7 DRS payload.

ST7-DRS PAYLOAD

ST7-DRS includes two main elements: an alternate set of drag-free control laws implemented on a separate computer, and an alternate micropropulsion system based on a novel colloid microthruster technology. During phases of the LPF mission where ST7-DRS operated, NASA's colloid thruster were used in place of ESA's cold-gas thrusters to move and orient the spacecraft, with the DRS control laws replacing the ESA control laws. During ST7 operations, the rest of the LTP payload played the same role as during the LTP-led parts of the mission, by providing information on the positions and attitudes of the test masses and applying forces and torques to the test masses, as requested by the DRS controllers. The DRS consisted of four major sub-systems to achieve spacecraft attitude control, drag-free operations and nanometer spacecraft position control using the gravitational reference sensor on the LTP. It included the colloid micronewton thrusters (CMNT) [3], Dynamic Control System (DCS) [5,6,7] the Integrated Avionics Unit (IAU) and the command and data handling flight software (C&DH FSW). The CMNTs were manufactured by Busek (Natick, MA). The DCS software was written at NASA's Goddard Space-

flight Center (GSFC) and the FSW was written at JPL. The IAU was manufactured by Broadreach Engineering (Phoenix, AZ). The sub-systems were integrated into 3 units that included the Electronics Assembly (EA) and two identical Colloid Micronewton Thruster Assemblies (CMTAs), also referred to as clusters. The Electronics Assembly consisted of the Integrated Avionics Unit (IAU) and a connector panel. The IAU interfaced with the primary LPF computer, known as the On-board Computer (OBC) and the OBC provided interfaces to the LTP instrument and other spacecraft systems such as the star tracker and communications systems. In drag-free operations, the LTP provide measurements of the position and attitude of the two test masses, which are processed by the OBC and sent to the IAU along with the spacecraft attitude measurements derived from the LPF star trackers. This information was processed by the Dynamic Control System (DCS) software running on the IAU, which determined the appropriate forces and torques to apply to the spacecraft and the test masses. Test mass force/torque commands are sent by the IAU to the OBC, which relays them to the front-end electronics within the LTP. Spacecraft force/torque commands are decomposed into individual CMNT thrust commands, which are then sent to the CMNTs. The two thruster assemblies contained four CMNTs each and their corresponding electronics. An exploded view of the LISA Pathfinder spacecraft with the ST7-DRS payload is in Figure 3. DRS was a unique payload in that during operations, it controlled the spacecraft attitude and another payload, the LISA Technology Package (LTP).

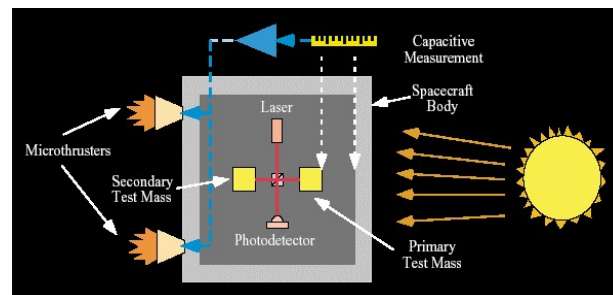


Figure 2. An illustration of the DRS concept. [3]

Colloid MicroNewton Thrusters (CMNTs)

The two Colloid Micronewton Thruster Assemblies (CMTAs) are identical units provided by Busek Co., Inc. A single unit with four thrusters is shown in Figure 3 with a functional block diagram. A thruster assembly includes: 4 thruster heads, 4 propellant feed systems, 4 Power Processing Units (PPUs), 1 cathode, and 1 Digital Control Interface Unit (DCIU). [3] The thruster head and feed systems are independently controlled through the PPUs, which are controlled, in turn by the DCIU. The DCIU has a power, command, and telemetry interface to the IAU. The DCIU also controls the cathode neutralizer. The DCIU has an on-board PROM (programmable read-only memory) that stores the thruster operating software and control algorithms. The CMTA mass is 14.8 kg. The nominal power for the CMTA 1 and 2 are 16.5-17.1 W, with a maximum power of 24.6 and 25.4, respectively, when heaters are operated at full power. Each thruster head includes a manifold that feeds nine emitters in parallel, a heater to control propellant temperature and physical properties, and electrodes that extract and accelerate propellant as charged droplets. The propellant is the room temperature liquid salt, an ionic liquid 1-ethyl-3methylimidazolium bis(trifluoromethylsulfonyl)imide (EMI-Im). The thruster electrical schematic is shown in Figure 4. The thrust from each head can be throttled from 5 to 30 μN by changing the beam voltage (2000-8000 V) and/or the propellant flow rate that determines the beam current (2.25-5.4 μA). Independent, fine control of both the beam voltage and beam current allow for precise control of thruster to better than 0.1 μN resolution with $<0.1 \mu\text{N}/\sqrt{\text{Hz}}$ thrust noise. The nominal specific impulse is 240 s. Propellant is stored in four electrically isolated steel bellows compressed by four constant force springs set to supply four microvalves with propellant at approximately 1 atm of pressure. The microvalve is piezo-actuated (developed at Busek) using $\sim 1 \text{ mW}$ of power to control the propellant flow rate and current to better than 1 nA. This level of precision corresponds to $\leq 0.01 \mu\text{N}$ of thruster, with a response time over its full range of less than 0.5 s. [8] Limits on analog

to digital converters and telemetry bandwidth brought the resolution down to 6 nA, corresponding to about 0.1 μN of thrust on orbit, but the ultimate capability is expected to be higher. The thruster performance requirements and performance during ground tests and operations in flight are summarized in Table 1.

The cathode neutralizer developed by Busek is made from carbon nano-tube (CNT) base with an extractor electrode. [9] The cathode is capable of producing 10 μA to 1 mA using extraction voltages of 250 to 800 V. One CNT cathode was tested in an ultra-high vacuum chamber for over 13,000 hours at 100 μA without incident. CNT cathodes have also been tested successfully with operating thruster heads during the pre- and post-dynamic tests and in each full functional test during the thermal environment qualification tests for each unit. Cluster 1 cathode demonstrated 13 μA at 242 V and 23 μA at 268 V in TVAC testing before flight. Cluster 2 cathode demonstrated 13 μA at 375 V and 26 μA at 420 V.

The thruster electronics includes 4 power processing units (PPUs) and one digital control and interface unit (DCIU) for each cluster. The PPU includes the high-voltage DC-DC converters that have been specifically designed and tested for this application by Busek Co. The DCIU controls all four thrusters and provides the command and telemetry interface to the spacecraft and DRS flight computer. The thruster control algorithm with the thruster performance model run in the DCIU to receive thrust commands and voltage and current telemetry to determine and send the next voltage commands to the PPU. The DCIU can also operate in a pass-through mode with voltage commands determined by the control algorithm running in the flight software in the IAU instead, as was demonstrated during the LISA Pathfinder Mission.

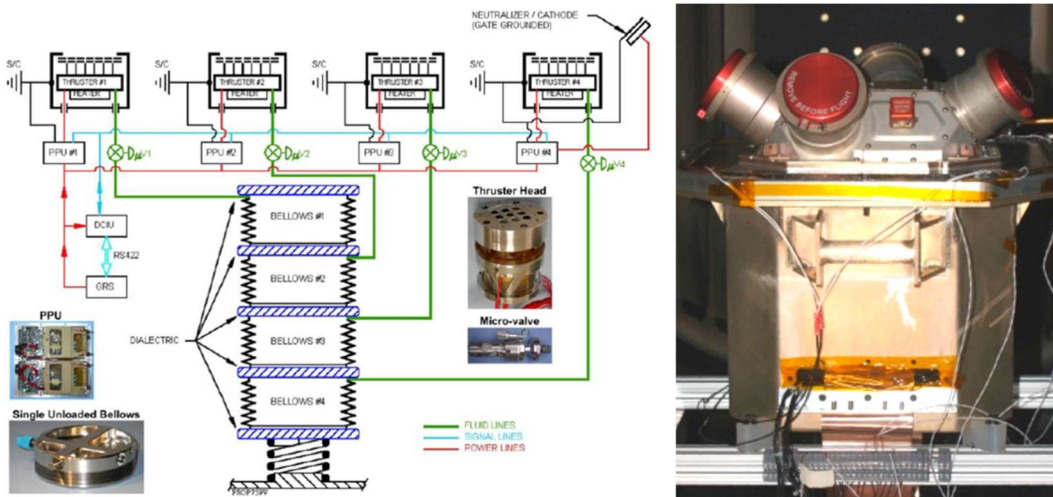


Figure 3. CMNT cluster functional block diagram [10] with pictures of various components (left) and the Busek Colloid Micro-Newton Thruster (CMNT) Flight Cluster 1 including four thruster heads, electronics, and cathode neutralizer (visible) in thermal-vacuum environmental test setup (right) [3].

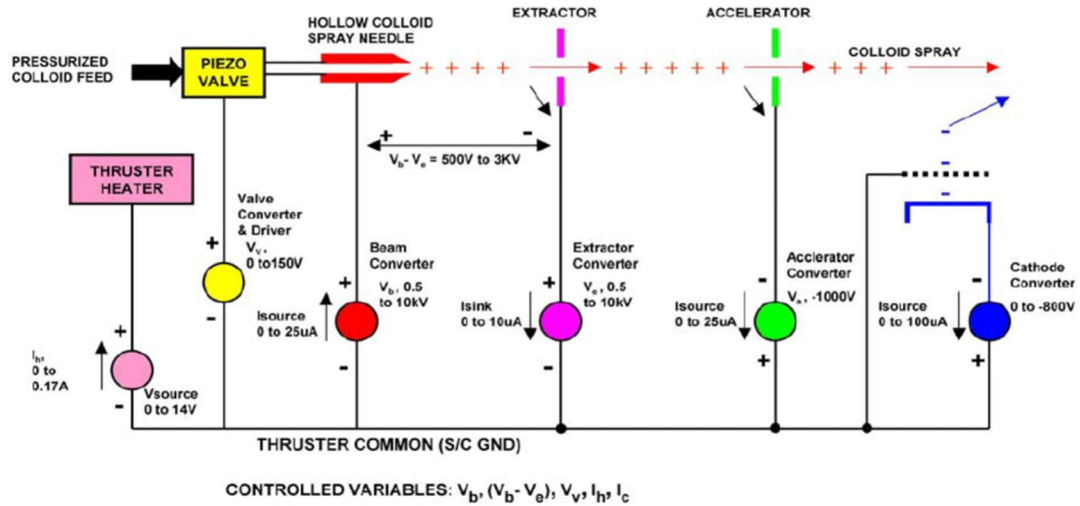


Figure 4. Thruster electrical schematic showing beam, emitter, extractor, accelerator, and cathode neutralizer voltage sources. [10]

Table 1. CMNT performance requirements and performance summary on the ground using an engineering model (EM) and in flight on all 8 flight units.

Performance Parameters	ST7 Requirement	Ground Tests (EM)	Demonstrated in Flight							
			Thr 1	Thr 2	Thr 3	Thr 4	Thr 5	Thr 6	Thr 7	Thr 8
Thrust Range (μN)	5 to 30	4.35 to 35.8	5-30	5-50	5-30	5-30	5-60	5-30	5-30	5-30
Thrust Precision (μN)	≤ 0.1	0.08 (0.01 calculated)	≤ 1	≤ 0.1	≤ 0.1	≤ 0.1	≤ 0.1	≤ 0.1	≤ 0.1	≤ 0.1
Thrust noise ($\mu\text{N}/\sqrt{\text{Hz}}$)	≤ 0.1	≤ 0.01 (3×10^{-5} to 3 Hz) <0.1 (3-4 Hz)	≤ 0.8	≤ 0.1	≤ 0.1	≤ 0.1	≤ 0.1	≤ 0.1	≤ 0.1	≤ 0.1
Thrust Range Response Time (s)	≤ 100 s	< 10 s	147 s	<10 s	<10 s	<10 s	<10 s	<10 s	<10 s	<10 s
Operational Lifetime (hours)	any measurable thrust on-orbit*	3478 hours during FLT 2B (245 Ns of impulse)	>2400 hrs (100 days)	>2400 hrs (100 days)	>2400 hrs (100 days)	1690 hrs, (70 days)	>2400 hrs (100 days)			
Propellant mass sprayed (grams)	none	113	74.8	67.02	84.1	68.89	64.46	59.05	91.07	89.52

* Given the unplanned 7+ years they sat, fully fueled after delivery. The mission lifetime requirement was 60 days for the nominal mission with a design goal of ≥ 2160 hours (90 days) to support an extended mission as well.

Dynamic Control System (DCS)

The flight software implementing the DRS Dynamic Control Software (DCS) algorithm resides in the IAU and was used to control the spacecraft and the test masses. It performed this function by computing thruster force commands to maintain spacecraft attitude and test mass force and torque commands for drag-free operation based on spacecraft attitude and test mass positions and attitudes received from the OBC. Its functions included sensor processing (from LTP and LPF), control filters propagation, actuation command generation (Thrust commands and electrostatic actuation commands) and internal fault notification. The on-board data handling (OBDH) of the OBC interacts with the DRS C&DH software on the IAU to pass commands and telemetry back and forth. The OBC stores ground commands on the MTL and telemetry from the DRS.

There are several DRS and DCS modes with different internal subsystem states within each mode. The DRS instrument enters a certain mode when the subsystems take on unique states within each mode. Each subsystem state may be commanded independently with the

configuration options presented in Figure. **Initialization/Safe Mode (Init or Safe)** is the mode the DRS instrument enters upon power being applied from the spacecraft. Only the IAU had power in this mode. This was also the instrument's Safe mode. **Standby Mode** was the mode in which the DRS was not controlling either the spacecraft or the LTP test masses, and its IAU and thrusters were on but disabled. Standby Mode was considered the initial mode for DRS operations. When the DRS thrusters are on and being commanded, they are commanded in one of two ways. In **Thruster Command Mode (ThrCmd)**, the thruster level of each thruster is directly commanded and the DCIU determines the operating current and voltage levels to comply with the command. **Thruster Diagnostic Mode (ThrDiag)**, as initially implemented, is a mode in which the DRS is not controlling either the spacecraft or the LTP test masses, its IAU and thrusters are on and enabled (thruster DCIU is on, PPU's are enabled) into diagnostic mode. This allows the thrusters to operate based on current and voltage commands (each thruster can be commanded independently) from the IAU. This mode was only expected to be used during commissioning phases or thruster fault diagnosis and recovery activities, but after a PROM anomaly in the DCIU, the mode implementation was adjusted to allow its use while the DRS was controlling the spacecraft, and then the mode was used for most of the rest of the mission.

When DRS is in control of the spacecraft, the DCS uses five control modes. **Attitude Only Control Mode (ATT)** stabilized the attitude of the spacecraft and the attitude and position of test masses after handover from the LPF without compensating for solar pressure. Both test masses had their position and attitude controlled in a "high force" (wide range) mode and the DCS test mass controllers were both in accelerometer mode. Spacecraft attitude was controlled by the micro-newton thrusters. **Zero-G Mode (ZG)** maintained spacecraft and test mass states while opposing solar pressure and other secular forces acting on the spacecraft using the micro-newton thrusters. Both test masses were either in high force (wide range) or low force (high precision) mode and the DCS test mass controllers were both in accelerometer mode to operate the test masses as accelerometers. Spacecraft attitude was also controlled by the micro-newton thrusters. This mode was used to measure thruster thrust levels by measuring the test mass motions and forces required to keep them in a fixed position and non-rotating in their housing. **Drag-Free Low Force (DFLF)** established drag-free motion about the reference test mass using the micro-newton thrusters. The reference test mass transitioned into Low-Force (high resolution) mode, with no electrostatic force commanding to control position (the spacecraft position was controlled around the reference test mass by the microthrusters and DCS), although small torque commands were used. **18 Degree-of-Freedom (18-DOF)** was the second drag-free mode and the highest control mode for the DRS, controlling all 18 degrees of freedom with the highest fidelity. This was the expected mode for "science" operations with the reference test mass freely floating and the spacecraft attitude stably controlled by the colloid thrusters. In this mode, drag free motion was to be maintained for two test masses along the sensitive axis and within the DRS bandwidth.

DRS Mission Mode	Spacecraft Control Mode	Reference Test Mass Control Mode	Reference Test Mass Force Mode	Non-Reference Test Mass Control Mode	Non-Reference Test Mass Force Mode
Standby	Standby	DFS Standby	N/A	DFS Standby	N/A
Attitude Control	Attitude-Only	DFS Accelerometer	High Force	DFS Accelerometer	High Force
Zero-G	Accelerometer				
Drag Free Low Force	Drag Free 1	DFS Drag Free 1	Low Force	Suspended Drag Free 1	Low Force
18-DOF Transitional					
18-DOF	Science	DFS Drag Free 2		Suspended Drag Free 2	
Zero-G LF	Accelerometer	DFS Accelerometer	Low Force	Accelerometer	Low Force

Figure 5. Table of DRS modes. [6]

The DCS provided both attitude and drag free control with the required performance with the colloid thrusters. It was required to maintain the spacecraft Z axis to an absolute accuracy of 2 degrees (3 sigma) half cone angle with respect to the Sun vector and the rotation around the Z axis to an accuracy of 2 degrees (3 sigma) with respect to the steering law. It was required to maintain the spacecraft position with respect to the test masses, about the sensitive axis (x-axis of the LTP housing frames H1 or H2), to better than 10 nm/ $\sqrt{\text{Hz}}$ in the measurement bandwidth (MBW). The measurement bandwidth covers the frequency range of 1 mHz to 30 mHz. The performance of the DRS in meeting all off the mission requirements is presented elsewhere [6,7] with this paper focusing on the performance of the CMNT thrusters.

THRUSTER PERFORMANCE AND CONTROL ALGORITHM MODELS

The DRS used a simplified version of the thruster performance model in the thruster control algorithm with 8 thrusters in a closed loop control with the DCS to control spacecraft attitude and spacecraft position and angles relative to the free-falling test masses. This section describes the thruster performance model, control algorithm and the simulation of it.

CMNT PERFORMANCE MODEL

The thrusters were controlled using the performance model in the thruster control algorithm. The functional form of the colloid thruster thrust model is given in Equation 1. [11] It provides the relationship between thrust level, T (microNewtons), the beam current, I_B (microAmperes), applied beam voltage, V_B (Volts), and thrust coefficient, C_1 , as defined in Equation 2. V_{tc} is a voltage drop across the Taylor cone jet between the emitter electrode at the beam voltage and the charged particle emission site. C_1 depends on the properties of the propellant in the α term, given in Equation 3, and multiple efficiency factors of the thruster (i.e. propellant utilization, grid impingement, beam spreading, and non-uniform charge-to-mass ratio distribution), where m/q is the charged particle charge-to-mass ratio and I_n is a single emitter current. The critical properties of the propellant depend on temperature and water content. They include propellant density, ρ , dielectric constant, κ , conductivity, σ , surface tension, γ , and a function, $f(k)$ that depends on the dielectric constant. The current supply efficiency, η_{curr} , is the ratio of the current of

charged particles in the beam to the current measured to the emitters. The grid current interception efficiency, η_{grid} , takes into account the beam current that is intercepted by the extraction electrode and does not produce thrust. The beam spread efficiency, η_{spread} , is the ratio of the actual thrust produced by the beam from an emitter to the ideal thrust from that beam if there was no beam divergence. The charge-to-mass-ratio efficiency, $\eta_{q/m}$, is related to the emitters producing charged particles with a distribution of charge-to-mass ratios that are accelerated to different velocities.

$$T = C_1 I_B^{\frac{3}{2}} (V_B - V_{tc})^{\frac{1}{2}} \quad (1)$$

$$C_1 = \frac{\alpha}{\sqrt{N}} \eta_{curr} \sqrt{\eta_{grid} \eta_{spread} \eta_{q/m}} \quad (2)$$

$$\alpha \equiv \sqrt{\frac{2}{I_n} \left\langle \frac{m}{q} \right\rangle} = \sqrt{\frac{\rho \kappa}{(f(\kappa))^2 \sigma \gamma}} \approx f(temp) \quad (3)$$

ST7-DRS used a simplified version of the performance model for thruster control that was validated on a thrust stand. The thrust, and the beam current and voltage were measured with an Engineering Model (EM) thruster horizontally supported on a magnetically levitated thrust stand with micronewton resolution [12]. Thrust was measured in the 5-30 μ N range to estimate the thrust coefficient, C_1 . The thruster was operated at room temperature, close to 25°C, and the propellant was dry to 150 PPM. The thrust coefficient C_1 was determined using the model in Equation 1 and setting V_{tc} to 0 V. The efficiency and V_{tc} terms were not fully characterized for the ST7 CMNTs prior to when the model needed to be finalized for drag-free controller and thruster controller design. With this simplified version of the performance model, the delivered thrust was achieved within 2% of the commanded thrust at nominal voltages, currents and temperature and with a C_1 of 0.0319. The nominal temperature was 25°C. The nominal beam voltage was 6000 V with a nominal range of 4000-8000 V. The nominal extraction voltage was 1600 V. The nominal current range was 2.25 – 5.3 μ A. At non-nominal voltages, Taylor cone losses and beam divergence effects can impact the thrust by <2% for beam voltages at 4000-8000 V. Taylor cone losses impact the thrust by $\leq 8\%$ for the full range of typically allowable beam voltages (2000-10000 V). Temperature also influences the value of α in C_1 , which decreases with increasing temperature. The values of C_1 at different temperatures have been predicted using models including the physical properties of the propellant and verified by measurement [13, 14]. This performance model was validated using a single thruster EM unit on a thrust stand, which was then used to verify that the 4 CMTA flight units in each cluster met requirements because they were too heavy for measurements on the thrust stand. The C_1 values estimated from ground measurements are 0.0372 at 15°C, 0.0343 at 20°C, 0.0298 at 30°C. They were used in the thruster control algorithm for the flight experiments at these temperatures.

CMNT CONTROL ALGORITHM AND MODEL SIMULATION

The thruster control algorithm was developed by Busek and Vtech Engineering Corporation. [8] The control algorithm was programmed into the PROM in the DCIU. A back-up copy of it was also programmed into the DRS C&DH flight software in the IAU, which was used instead for most of the mission after the Cluster 2 DCIU failed to process thrust command packets (an investigation into the root cause suggests a radiation effect damaged the local static PROM) but was still able to process enable/disable and diagnostic commands. The DRS Drag-Free Control Software resides in the IAU and is responsible for computing thruster force commands to maintain spacecraft attitude and test mass force and torque commands at 10 Hz for drag free operation based on the spacecraft attitude and test mass position and attitudes received from the On-Board Computer (OBC). The OBC resides on the LISA Pathfinder (LPF) spacecraft and acquires this telemetry from the LISA Technology Package (LTP).

The thruster control model translates high level thrust commands from the IAU into the low-level voltages required by the local Power Processing Units (PPU) to control the thrusters. It takes the measured current and voltages to calculate thrust level using the performance model, compares

it to the new thrust command and then calculates the new beam current, then beam voltage and then the propellant flow control voltage to command for each thruster. It limits the voltage and current ranges and the changes in them in each cycle. A flow diagram for the model is given in the Figure 6 [8]. It executes every 100 ms within 70 ms for all 8 thrusters. The objective of the algorithm is to drive the thrust error to zero as soon as possible by controlling the beam voltage and current. The thrust error is the difference between the thrust calculated using performance equation and measured beam current and voltage and the thrust command from the IAU. The algorithm also has a requirement to have the beam voltage converge to a nominal beam voltage, V_{BNOM} , to ensure that the thrusters are operating at an average voltage that allows both bidirectional headroom for the beam voltage adjustments and ensures that over the long term, the average specific impulse is at a desirable value.

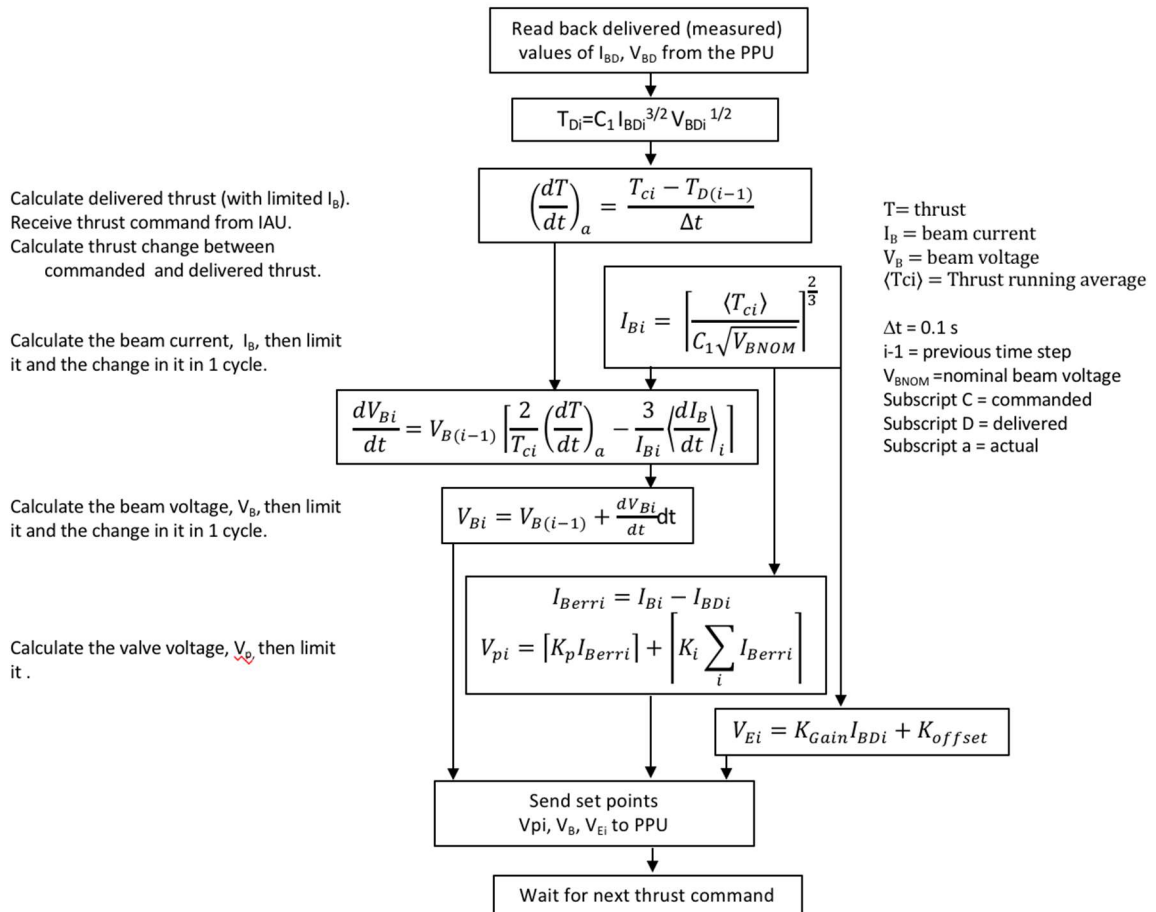


Figure 6. Primary elements of the CMNT control algorithm.

A model simulation was developed of the thruster control algorithm in the commercial Wavemetrics Igor data analysis tool to predict thruster performance and noise. It can be used to test potential improvements in various parameters in the control algorithm to improve the performance of the colloid thrusters and the DRS in flight to reduce the thrust noise on the spacecraft. This model follows the flow diagram and details shown in Figure 6. It uses the same data types and limited precision for the various controlled and monitored parameters as programmed into the DCIU and the DRS C&DH flight software. It includes nominal beam voltages and maximum and minimum voltage and current values. It includes maximum current and voltage step sizes per cycle (0.1 s). It includes proportional and integral gains on the piezo valve controller to control the mass flow rate of the propellant and the beam current. It also includes an anomalous

3 cycle timing delay in the telemetry that resulted from the control algorithm running in the FSW in the IAU instead of the DCIU, once that change was made early in the mission.

MODEL VALIDATION APPROACH

The performance and thruster control models were verified in flight with the DCS control models by meeting the mission control and performance requirements and then verified per thruster for all 8 thrusters by measuring the thrust from each thruster and using models of the DRS to estimate the thrust coefficients. A model simulation of the thruster control algorithm was developed to predict delivered thrust profiles for thrust command profiles to estimate thruster noise and study the impact of thruster anomalies and control algorithm changes on thruster noise. It was also validated against flight data and applied to show how the CMNT propulsion system noise performance was better than the 1 Hz telemetry data suggested and how it could be improved for future missions. This section of the paper discusses the approaches developed to validating the models with flight data.

PERFORMANCE MODEL VALIDATION APPROACH

The thruster performance model was validated before flight by measuring the thrust, beam current and beam voltage and verifying that they agreed within the required accuracy over the mission thrust range of 5-30 μN . Thrust measurements were taken on the ground with engineering model thrusters using a magnetically levitated thrust stand. The nominal thrust stand accuracy was 2% and the temperature control was accurate to within 2 degrees Celsius. As discussed in the previous section, at non-nominal voltages, Taylor cone losses and beam divergence effects impacted the thrust by <2% from the model prediction with a constant C_1 and V_{tc} set equal to zero for beam voltages between 4-8 kV and $\leq 10\%$ for the full range of typically allowable beam voltages (2-10 kV). Because of the closed loop spacecraft control approach with 8 thrusters, delivering the required thrust to within 10% was acceptable with 0.1 μN thrust control precision.

The thruster performance model was validated in flight by the DRS. The LISA Technology Package (LTP) inertial sensor was used to measure the delivered thrust level of each of the thrusters and verify the thrust model in flight. Because the test masses were not physically connected to the spacecraft, the LTP measured positions and actuation of the test masses could be used to estimate the forces and torques applied to the spacecraft [5,6,7]. This measured thrust was compared to the beam current and voltage and the performance model to estimate C_1 . Experiments were conducted for nominal current, voltage, and temperature, as well as for off-nominal values. Because the thrusters were simultaneously being used to control the spacecraft attitude, arbitrary injections were not possible in flight. Therefore, the bulk of experiments involved adding sinusoidal injections at several chosen frequencies above the bandwidth of the attitude controller and smaller amplitudes ($\sim 1 \mu\text{N}$), to allow good signal to noise while preserving system stability. In one experiment, the test masses were injected with position signals. The modeled thruster response compared to the measured response can be used to estimate the average C_1 for all of the thrusters.

CONTROL ALGORITHM AND MODEL SIMULATION VALIDATION APPROACH

The approach to validating the control model was to demonstrate that it could deliver the required thrust command profile expected and meet the thruster noise requirements and spacecraft attitude and position requirements. Acceptance tests were conducted before flight with expected thrust command profiles. These tests were done with thrust command profiles for the highest control mode expected in flight, which was the 18DoF mode. All 8 thrusters demonstrated approximately the required thruster noise level (difference between thrust calculated with the model and commanded thrust) for DC thrust commands of 0.1 $\mu\text{N}/\sqrt{\text{Hz}}$ during the ground tests with AC thrust commands. The control model was validated in flight in all of the DRS modes including

18DoF. In flight, the control model was validated by maintaining the required spacecraft attitude and position control in all of the DRS modes while meeting the thruster noise requirement of $0.1 \mu\text{N}/\text{Hz}$ in the 1-30 mHz frequency range.

The approach to validating the thruster control algorithm model simulation was to compare the thrust noise calculated from the thrust profiles predicted by the model with the thrust noise calculated from the flight thruster thrust profiles. The thrust noise was estimated by taking the Power Spectral Density (PSD) of the difference between the calculated and commanded thrust. The thrust is calculated from the current and voltage telemetry using the performance model. Thrust noise profiles were compared for different DRS modes in the validation process. Experiments were conducted to change various control algorithm parameters to show that the simulation could predict the results observed in flight. The simulation included a telemetry delay of 3 cycles (0.3 s) in the thruster parameters including beam current and voltage that resulted in voltage oscillations. This delay was a result of running the thruster control algorithm in the IAU instead of the DCIU after it was required because of a DCIU anomaly. The validated simulation was used to show the expected improvement in noise spectra without this and another flight anomaly. It can also be used to explore approaches to reducing thruster noise by improving the control algorithm.

RESULTS AND DISCUSSION

PERFORMANCE MODEL VALIDATION RESULTS

The thruster performance model, control algorithm and DCS control laws were verified by the DRS using them to maintain the required attitude and spacecraft position control in each of the DCS modes. Figure 7 shows several minutes of thrust command telemetry and calculated thrust as calculated from the thruster beam voltage and current telemetry using the thruster performance model. The spacecraft attitude errors and test mass position and angles are in Figure 8. The attitude error requirement was 2 deg (35 millirad). The test mass position requirement was $10 \text{ nm}/\sqrt{\text{Hz}}$ at 1-30 mHz. The bump in the data is suspected to be a micrometeoroid impact and is included in these figures to show a higher transient command case. Figure 7 shows that the thrusters and DCS responded to the disturbance and the thruster thrust level (markers) followed the thrust commands (solid lines) very well. Figure 6 shows that the DRS maintained the spacecraft position and attitude requirements, even during a significant disturbance in 18DoF. The spacecraft position was temporarily displaced by about 150 nm from the impact.

The LISA Technology Package (LTP) inertial sensor was used to measure the delivered thrust level of each of the thrusters and verify the thrust model in flight. It was used to measure the position and attitude of the test masses for calculations of the forces and torques applied to the spacecraft. Figure 9 presents both the thrust level predicted along the 3 axes ($T6_CMNT_{x,y,z}$) as calculated from the current and voltage measurements using the thruster model, and the thrust level calculated using the averaged data from both of the gravitational reference sensors ($T6_GRS_{x,y,z}$) in flight, for comparison. The agreement demonstrated was sufficient for the DRS to achieve the required noise performance for LISA Pathfinder. These thruster functional test data were collected during commissioning with ESA cold gas thrusters in operation that contributed to the noise in the measurements. The x-axis measurements were acquired with greater sensitivity and less noise using the optical interferometer, as shown in Figure 9. The measurements on the y and z axes were made with the electrostatic metrology system.

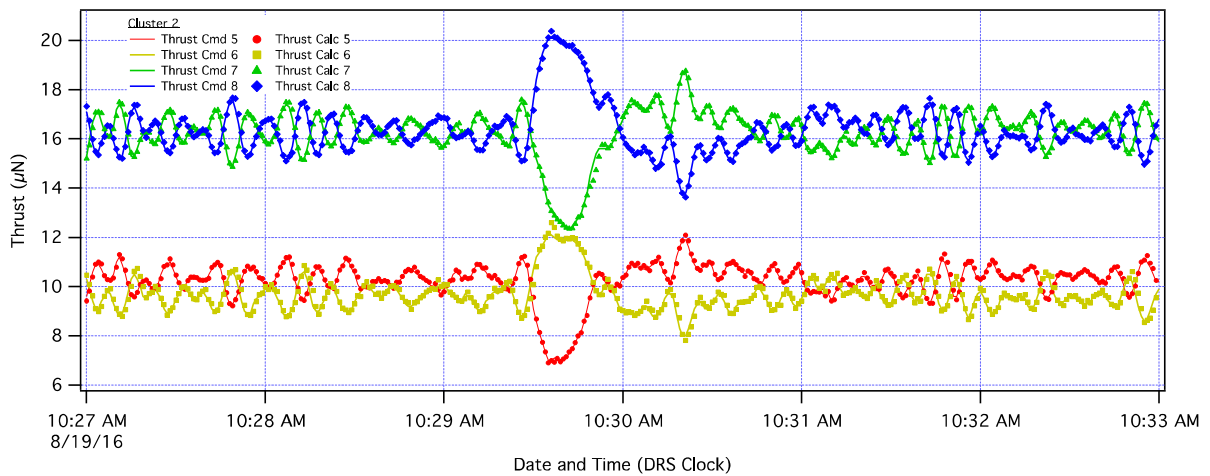
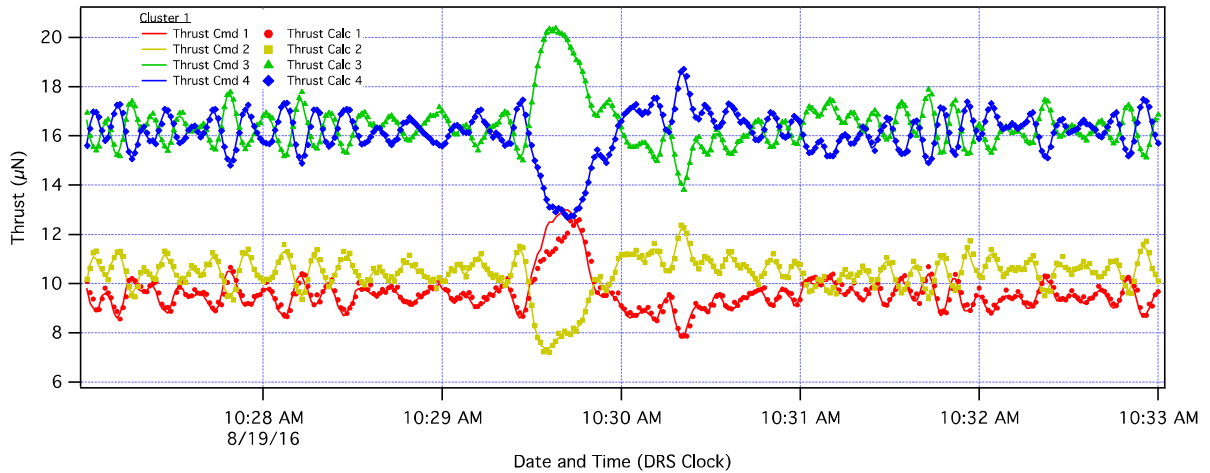


Figure 7. Thruster command (Solid line) and calculated (markers) thrust levels, validating the performance model and control algorithm in the flight demonstration of spacecraft attitude and drag-free test mass position control in 18DOF with a suspected micrometeoroid impact to the spacecraft on DoY 232 (August 19, 2016).

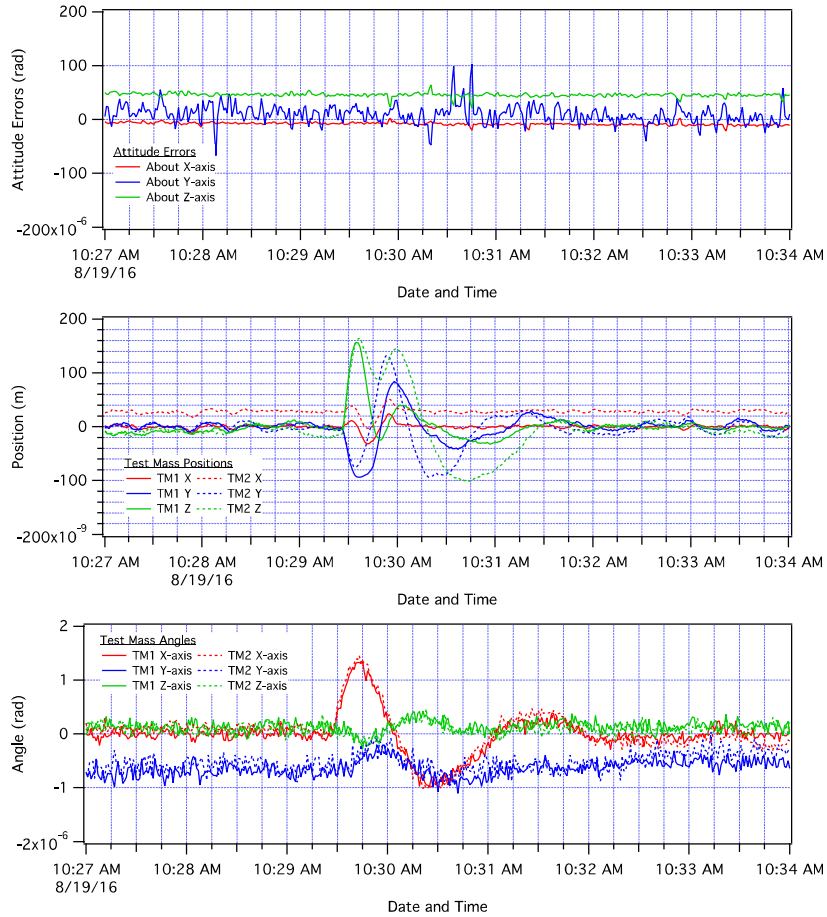


Figure 8. Spacecraft attitude error, and test mass position and angles validating the performance model and control algorithm in the flight demonstration of spacecraft attitude and drag-free test mass position control in 18DoF with a suspected micrometeoroid impact to the spacecraft DoY 232 (August 19, 2016).

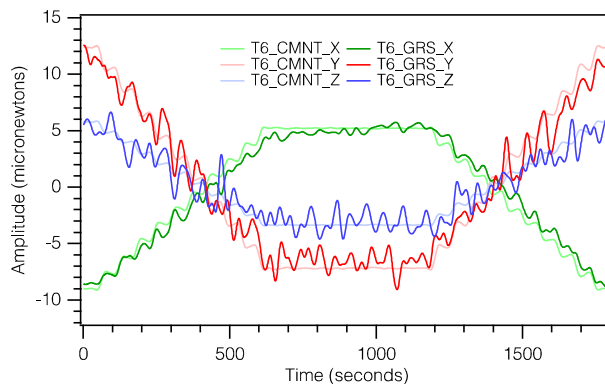


Figure 9. Thruster 6 thrust on x, y, z axis calculated using thrust model and current and voltage measurements and using the spacecraft gravitational reference sensor (GRS) to measure thrust. Data shows good agreement between calculated and measured thrust.

Multiple experiments were conducted to measure thrust using the LTP sensor to further validate the thruster performance model by measuring thrust to verify the C_1 value for the thruster performance model. While the DCS was in a Zero-G mode, one thruster at a time was injected with 3 or 5 μN , and 23, 29, and 40 mHz sinusoidal thrust signals on top of the DCS thrust levels

commanded. Using the thruster performance model with the measured thrust and beam current and voltage, the thruster constant C_1 was estimated for the measured thrust. These injections were also done at different temperatures for all 8 thrusters to investigate how C_1 changed with temperature in comparison to estimated values from models and ground measurements before flight. The results are presented in Table 2. The table includes the C_1 values estimated from the thrust stand (T/S) measurements and from the thrust measurements on the spacecraft. During the primary mission these experiments were conducted in a high force accelerometer (Zero-G) mode. A low force accelerometer mode was added before the primary mission because it improved the position measurement precision. It further improved the measurement precision to only measure position along the x-axis because of the interferometer measuring position along that axis. The thruster signal injections were then repeated for all of the thrusters. The results of this experiment are in Table 3. The results from this experiment conducted multiple times during the primary and extended mission are included in the graphs in Figure 10. The results show that the C_1 estimates from thrust measurements in flight are lower than the estimates from thrust measurements on the thrust stand by as much as 10%. C_1 estimates are given for all 8 of the thrusters. They are very similar for all of the thrusters, but vary by <5% percent from their average value estimated. Relative changes in C_1 with temperature agreed within 1.5% of pre-flight estimates and those used in the flight experiments. A graph of the C_1 estimates from the flight experiments is included in Figure 10 with markers and dotted lines. The graph shows the average value for all of the thrusters as the solid line. The results show that C_1 varies with thruster operating conditions and that the thrust level in flight could have been 10% lower than was predicted with the performance model and the C_1 value of 0.0319. Despite this difference, the DRS still met the performance requirements because of the closed loop control. V_{tc} was estimated for the thrusters as a function of current to include in the performance model to determine if it would result in less variation among thruster C_1 values. The results showed that it did not reduce the dispersion in these values. Months of operations were conducted successfully with a C_1 value of 0.0287 and several months were conducted with a value of 0.0319. These results suggest that the thruster C_1 values varied in flight and were different from the value estimated from ground measurements by several percent and it was acceptable in the closed loop control DRS.

Table 2. C_1 values estimated for each of the thrusters from the thrust, beam current and beam voltage measurements on the spacecraft at different temperatures.

Thr	$C_1 \times 1000$ 15°C	+/-	$C_1 \times 1000$ 20°C	+/-	$C_1 \times 1000$ 25°C	+/-	$C_1 \times 1000$ 30°C	+/-
T/S	37.2		34.3		31.9		29.8	
1	36.7	0.1	35.2	0.09	30.8	0.08	29.2	0.08
2	35.2	0.07	31.8	0.07	29.9	0.06	27.9	0.06
3	35.0	0.07	30.9	0.06	30.0	0.06	28.1	0.06
4	37.4	0.08	33.8	0.07				
5	35.4	0.07	32.1	0.07	30.7	0.06	28.0	0.06
6	35.5	0.08	32.5	0.07	29.7	0.06	27.7	0.06
7	37.1	0.08	33.4	0.07	31.3	0.06	28.5	0.06
8	37.1	0.08	33.8	0.07	30.6	0.06	27.9	0.06
AVG	36.2		33.0		30.5		28.2	

Table 3. C1x1000 values estimated for each of the thrusters from the thrust, beam current and beam voltage measurements on the spacecraft at 25°C.

Thr	C1x1000	+/-	Delay	+/-
T/S	31.9			
1	31.9	0.1	-0.48	0.02
2	30.9	0.1	-0.25	0.02
3	32.1	0.1	-0.12	0.01
4				
5	31.5	0.1	-0.13	0.02
6	30.9	0.1	0.02	0.02
7	30.4	0.1	-0.33	0.02
8	30.5	0.1	-0.48	0.02
Avg	31.2			

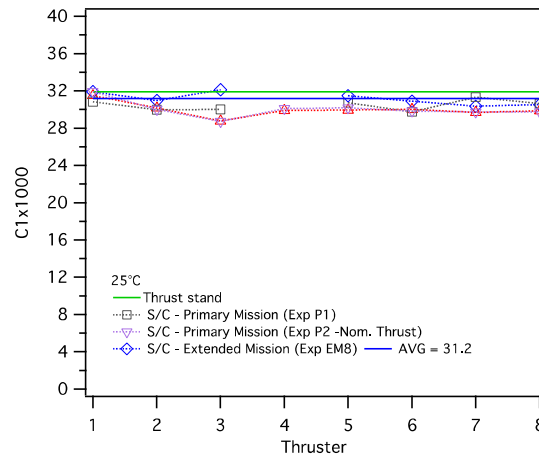


Figure 10. C1x1000 values estimated from thrust measurements on the spacecraft the same temperature during experiments throughout the primary and extended mission.

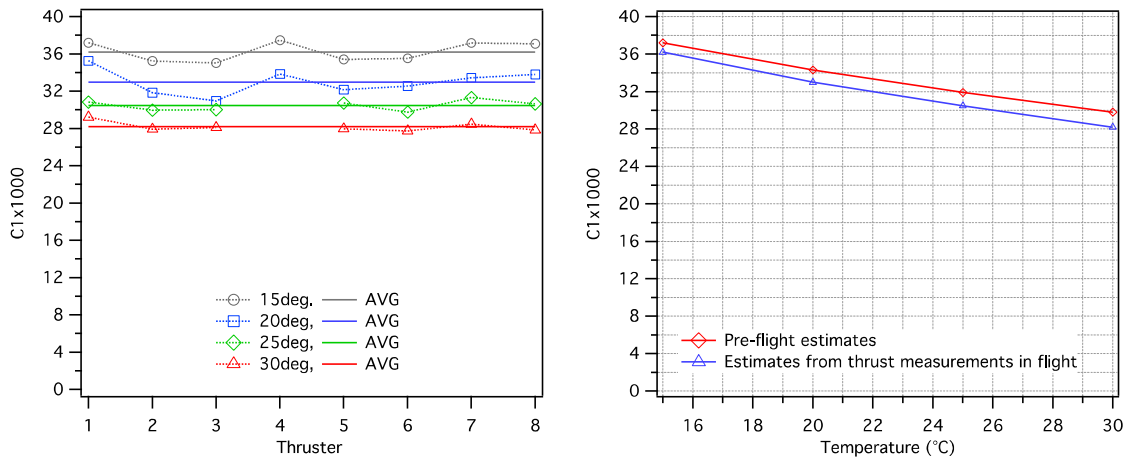


Figure 11. C1x1000 values estimated from thrust measurements on the spacecraft at different temperatures.

CONTROL ALGORITHM MODEL VALIDATION RESULTS

The control algorithm was validated in ground tests and in flight. It was validated on each of the eight thrusters during thruster cluster acceptance testing. The thrust command and calculated thrust data are in Figure 11 for thruster 1. The thrust was calculated from beam voltage and current telemetry using the thruster performance model. The thruster was commanded with 18DoF mode thrust profiles that were expected in flight for about 30 minutes of the acceptance test. Thruster commands were sent at 10 Hz and thruster telemetry was received at 10 Hz. Figure 12 shows commanded and calculated thrust profiles for thruster 1 in the graph on the left. The data looked similar for the other thrusters. The graph on the right in Figure 12 shows the power spectral density (PSD) of the thrust noise that was calculated for thrusters 1,2,3,4 in thruster cluster 1. The thrust noise in this analysis is calculated as the difference between the commanded and delivered thrust. The graph shows that all of the thrusters had very similar thrust noise for an AC thrust profile. The requirement on a DC thrust profile was $0.1 \mu\text{N}/\sqrt{\text{Hz}}$ in the 1-30 mHz frequency band. Thruster noise for an AC thrust profile almost met the requirement. The noise on a DC thrust command profile was expected to be much lower.

The control algorithm was validated in flight in all DRS modes by meeting the DRS performance requirements. The validation data for meeting spacecraft attitude and test mass angle and position in 18DoF on DoY 115 with the thruster performance model and the control algorithm are in Figure 6. Figure 12 shows thrust command profiles for two thrusters that are similar to DC command profiles from DoY 254 in Zero-G mode. This figure shows both 1 and 10 Hz telemetry. Thruster 1 blips to a higher thrust level every ~ 4 s, depending on the current level, because of one of the nine emitters was blipping on and off. There is also noise on the calculated thrust for each of the thrusters because of a telemetry delay of ~ 3 cycles (0.3 s) that resulted from a DCIU anomaly [4] that required the thruster control algorithm to run in the flight software in the IAU instead of the DCIU. The frequency of that noise is ~ 600 -700 mHz. The amplitude is $0.4 \mu\text{N}$, or $\pm 0.2 \mu\text{N}$ from the commanded thrust level. When the telemetry is sampled at only 1 Hz, the frequency of that noise appears to be ~ 0.3 Hz. Figure 14 shows the thrust noise PSD for that same time over a longer period on DoY 254 in Zero-G mode. The thrust noise PSD is shown for 7300 s of 1 Hz data and 200s of 10 Hz data. The DRS control and thruster algorithm ran at 10 Hz. The thruster telemetry was nominally received at 1 Hz. A sequence was run to collect only 200 s of 10 Hz data. These data verify the noise requirement of $0.1 \mu\text{N}/\sqrt{\text{Hz}}$ in the 1-30 mHz frequency band. The noise calculated from the 1 Hz telemetry meets the requirement. The noise estimated from the 200 s of 10 Hz data shows that it is below the requirement. Figure 14 shows that sampling the thruster telemetry at only 1 Hz causes sample aliasing that suggests higher noise and at lower frequency that it actually is. It causes the noise in the band of our requirement to be much higher. The 200s of 10 Hz data also shows that the noise created by the blipping thruster 1 emitter and the noise created by the telemetry delay was not in the requirement frequency band and do not affect the DRS in meeting performance requirements. Unfortunately, there is only 200 s of the 10 Hz data, which makes the PSD on the 10 Hz data unreliable below 20 mHz. However, in the Zero-G mode, the noise meets the $0.1 \mu\text{N}/\sqrt{\text{Hz}}$ at 1-30 mHz to validate the control algorithm and the DRS. Figure 14 shows thrust command and calculated profiles before the DCIU anomaly and telemetry delay. The noise on the calculated thrust has an amplitude of only $0.1 \mu\text{N}$ instead of $0.4 \mu\text{N}$. The PSD of the noise in Figure 15 shows that the thrust noise was significantly lower for all thrusters without the delay, including thruster 1.

The thruster noise was also characterized in 18DoF to validate the control algorithm for that DRS mode. Calculated and commanded thrust profiles are shown in Figure 5 for a period in 18DoF. The thrust command profile has much more variability in 18DoF than in Zero-G. Figure 5 shows that the thrust level follows the command very well, except for thruster 1. It also has a delayed response time in comparison to the other thrusters throughout the entire mission. Figure 12 shows that it did not have this issue during acceptance testing. Thrust noise PSD is shown for 18DoF mode on DoY 115 in Figure 16. The thrust noise data in the graph on the left was calculated from 1 Hz telemetry that was obtained throughout the mission. The data in the graph on the right was calculated from 200 s of 10 Hz data immediately after the 1 Hz data, showing much lower

noise without the aliasing issue. These data in the graph on the left in Figure 16 show that all of the thrusters almost met the requirement at 1-30 mHz except for thruster 1. The data on the right, suggests that they may all have also met the requirement. The data in Figure 16 shows that the thrust noise of all of the thrusters is very similar. 18DoF mode was the most demanding DRS mode for the thrusters and resulted in the highest thrust noise for all of the modes. The thrust noise in the other modes was lower. The thruster noise in ground testing before flight was different across the frequency displayed; However, they were very similar in the 1-30 mHz frequency band requirement. The data shows that the thruster noise in flight was lower than the noise estimated from the ground test data. Characterizing the thrust noise in 1-30 mHz frequency band required several thousand seconds of thruster telemetry. Telemetry was only provided at 1 Hz for the duration of the mission. The graph on the right in Figure 15 presents the thrust noise calculated from the 10 Hz thruster telemetry that is only available for 200 s. It includes the peak at ~250 mHz in the thruster 1 noise spectra from the blipping emitter. At lower frequencies, the noise is below the requirement. Because only 200 s of data were taken at 10 Hz, the noise spectra is only credible down to about 20 mHz. What the data shows is that the noise spectra is being aliased down to lower frequencies when only sampled at 1 Hz instead of 10 Hz. It suggests that even thruster 1 meets the noise requirement in the 1-30 mHz frequency band; However, we cannot verify it without thousands of seconds of 10 Hz thruster telemetry. Noise aliasing artificially increased the noise of the other thrusters also in the 1 Hz telemetry data. There was a thruster telemetry delay of about 3 cycles that resulted from running the thruster control algorithm from the IAU instead of the DCIU that caused the beam voltage to oscillate around the commanded value. The oscillation was observed with a period of about 1.3 s in the 10 Hz data, producing a noise peak at ~650 mHz in the noise spectra. It was observed with a period of ~4 s in the down-sampled 1 Hz thruster telemetry and at about 250 Hz in the noise. As shown in Figure 16, the down sampling of the thruster telemetry resulted in aliasing that produced artificially higher noise in the noise spectra in the required band. These results suggest that the two anomalies during the mission that increased the thruster thrust noise spectra, did not increase it in the required frequency band and therefore, did not affect the performance of the DRS in meeting the mission requirements. The model of the thruster control algorithm is valuable in suggesting the thrust noise spectra without these sources to consider for future missions with these thrusters.

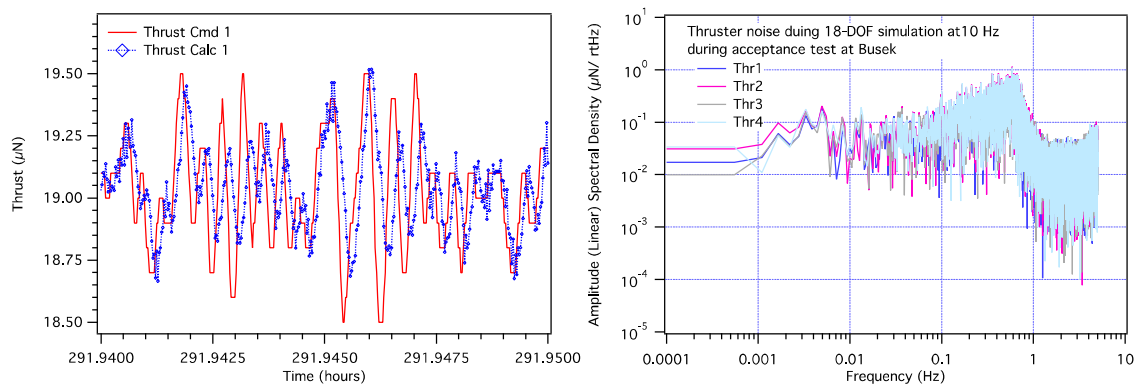


Figure 12. Thrust command and calculated profiles and thrust noise during thruster acceptance tests at Busek which validate the thruster control algorithm.

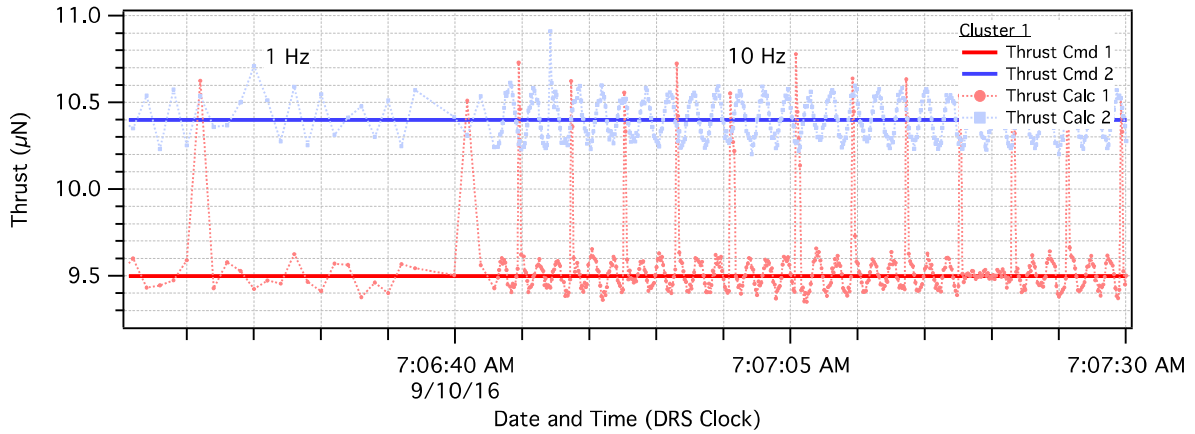


Figure 13. Command and calculated thrust profiles for thrusters 1 and 2 on DoY 254 (September 10, 2016) in Zero-G mode. The beam voltage is oscillating in the DCIU pass through mode causing most of the noise in data.

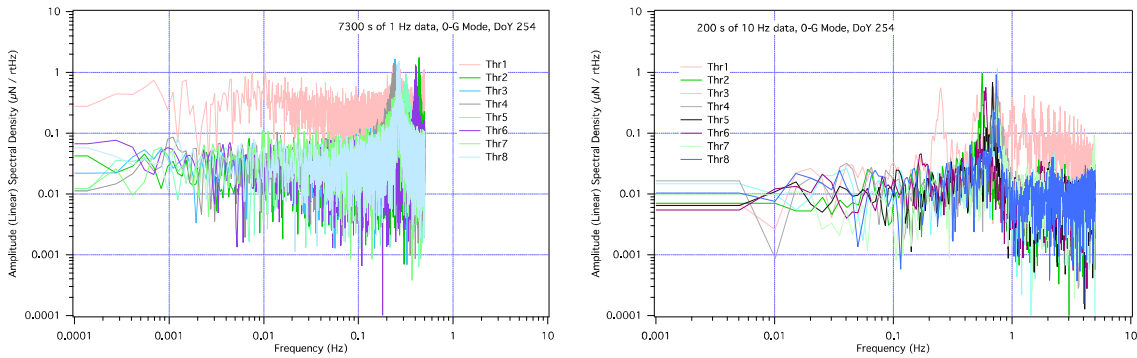


Figure 14. Thrust noise calculated from 1 and 10 Hz flight telemetry data for all 8 thrusters on DoY 254 2016 (September 10, 2016) in Zero-G mode showing that higher frequency noise (only observable with 10 Hz data) is artificially aliased into the 1 Hz data.

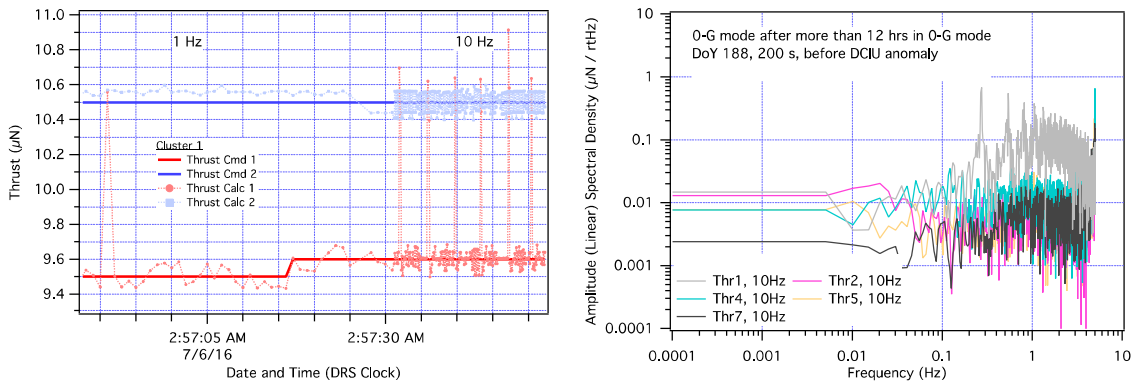


Figure 15. Command and calculated thrust profiles for thrusters 1 and 2 on DoY 188 (July 6, 2016) in Zero-G mode before the DCIU anomaly.

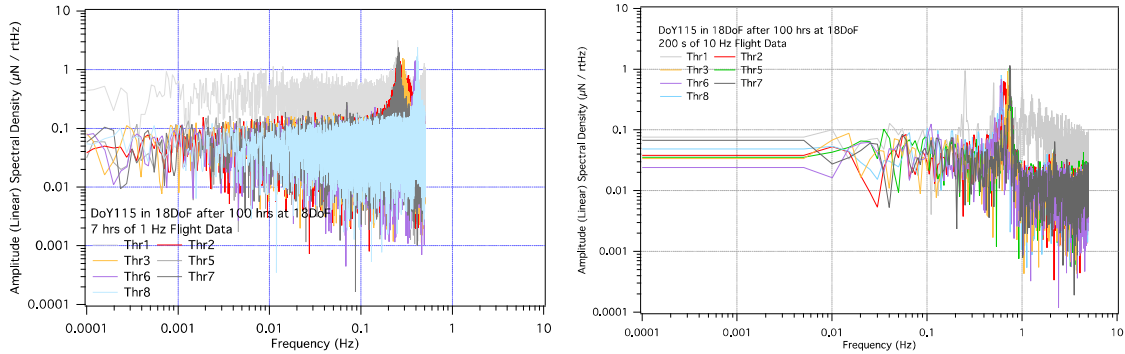


Figure 16. Thrust noise calculated from 1 and 10 Hz flight telemetry data for all 8 thrusters on DoY 115 (April 25, 2017) in 18DoF mode.

The thruster control algorithm model was verified using both 1 and 10 Hz flight thruster telemetry and then applied to suggest what the noise spectra could have been in flight where it was not measured. Figure 17 shows thruster 5 thrust noise calculated from flight telemetry and from thruster control algorithm simulation results using the same thrust command telemetry from flight. Thruster noise PSD 1 was calculated from the 1 Hz thrust command and calculated telemetry. Thruster noise PSD 2 was calculated from simulation results using the same thrust command telemetry. The simulation runs at 10 Hz. The 1 Hz thruster command telemetry had to be interpolated to populate a 10 Hz thrust command profile. The noise analysis was done on a 1 Hz sampling of the difference between the calculated and commanded thrust to create the thrust noise PSD 2. The agreement between PSD 1 and 2 provides model validation. The thrust noise PSD 3 was created from the 10 Hz simulation results from the same data to show what it could look like if we had 10 Hz telemetry for the 7 hours instead. The thruster noise PSD 4 was generated from 200 s of 10 Hz flight data taken immediately after the 7 hours of 1 Hz data. The noise PSD 5 is the result from the simulation of the same 200 s of 10 Hz flight thrust command telemetry. These two results further validate the simulation. The noise PSD 1-5 all include the 3-cycle delay in the thruster telemetry in the thruster control algorithm simulation that produces the peak at 0.7 s in the 10 Hz data and is aliased down to lower frequencies and spread out in the 1 Hz telemetry noise. Thruster noise PSD 6 is the result of running the simulation on the 7 hours of thrust command telemetry without the 3-cycle delay from the flight anomaly in the DCIU. This result suggests that the CMNT thrust noise could be significantly lower than was the analysis results suggest on the available telemetry. It also suggests what thruster 1 noise could have been without both the blipping emitter and DCIU anomalies. The simulation results suggest that the thruster noise was much lower than originally reported [4] and could be more than 10X lower than requirements without the anomalies.

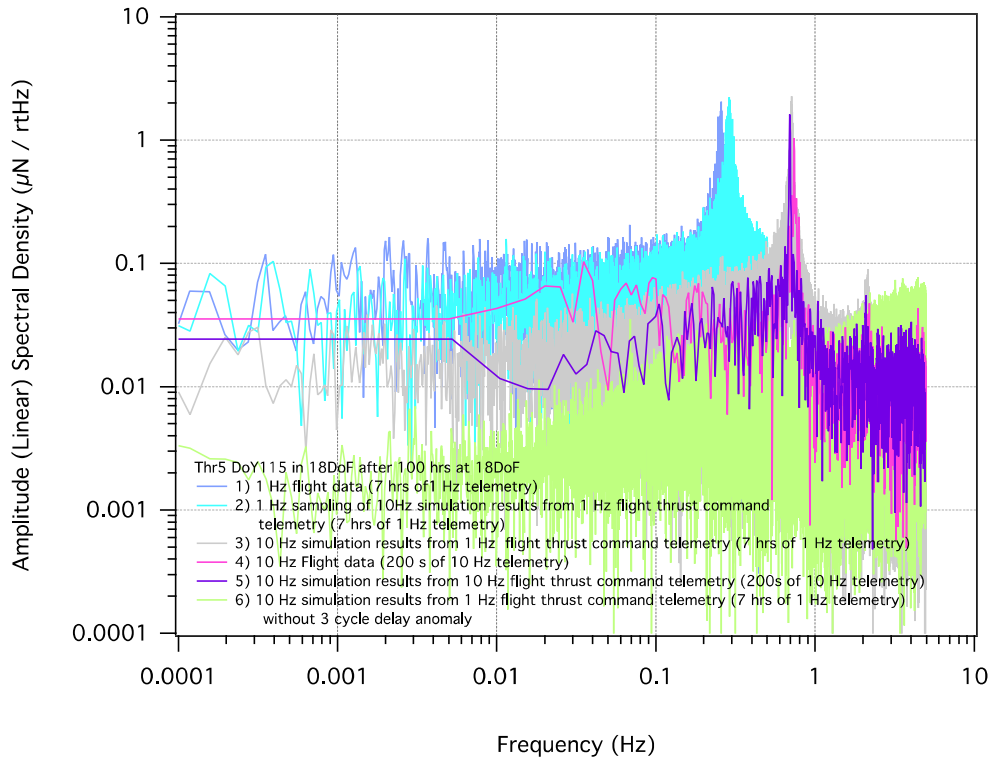


Figure 17. Thruster 5 noise calculated from flight data and from the algorithm simulation results

SUMMARY AND CONCLUSIONS

The ST7-DRS mission demonstrated CMNT and drag free spacecraft control on the LISA Pathfinder spacecraft and validated the thruster technology, performance model and control algorithm in flight for the first time. The DRS met the performance requirement for the mission in providing LPF spacecraft attitude and drag-free control within position, attitude and thrust requirements. The thrust noise requirement was $0.1 \mu\text{N}/\sqrt{\text{Hz}}$ at 1-30 mHz. The performance of all eight CMNTs in flight were consistent with performance during acceptance testing on the ground, except thruster 1. Thruster 1 had one of the 9 emitters blipping on and off. Thruster 1 also had a slower response time, which is currently under investigation. All of the thrusters demonstrated the thrust range of 5-30 μN with the required response time and precision, except thruster 1 did not meet the response time requirement. Thrusters operated over 2400 hrs (100 days) in flight. Individual thruster thrust was measured in several experiments over eight months using the gravitational reference sensor on the LPF. The results suggest that the thruster coefficient, C_1 , is lower than measurements on the ground suggested. It was lower by as much as 10%. It was lower on average for all of the thrusters by <6.5%. The variation in C_1 among all eight thrusters throughout the mission was <5% at 25°C. The relative changes in C_1 with temperature agreed with pre-flight estimates to within 1.5%. These variations in C_1 resulted in lower thrust levels in flight by as much as 10% and it was acceptable in the mission because of the closed loop spacecraft control, thrust precision and thrust noise.

The thruster control algorithm was validated in flight also with the DRS meeting the mission thrust noise requirement. Meeting this requirement and characterizing thrust noise is important because the micro thrusters are considered to contribute the largest component of noise on the GRS for measuring gravitational waves. The thrust noise measured in flight was lower than the measurements on the ground in a simulated 18DoF mode. Measurements in flight validate the control algorithm in meeting the noise requirement in the Zero-G mode. They also suggest that it

was met in 18DoF mode also, however, 10 Hz data over several thousand seconds was required for direct validation and those data were not available. Instead, models validated with 10 Hz data showed that calculated thrust at lower frequencies did meet requirements. The DCS and thruster control algorithm ran at 10 Hz. Thruster telemetry was available at only 1 Hz, except when a sequence ran to collect 10 Hz telemetry for 200 s. There were two DRS anomalies that increased thrust noise: thruster 1 had a single emitter blipping on and off at about 250 mHz, depending on the current level, and a telemetry delay after a DCIU anomaly [4] caused beam voltage oscillations with a frequency of ~650 mHz. These sources of thrust noise contributed to it beyond the measurement band of 1-30 mHz, therefore, they did not affect the system performance in band or prevent it from meeting performance requirements.

A model simulation of the thruster control algorithm was validated with flight data and as a tool to predict CMNT thrust noise. The model simulation was developed in a commercial Wavemetrics Igor data analysis tool. It was used to predict thrust noise at critical frequencies where flight data was not available. It was validated with 1 Hz and 10 Hz flight thruster telemetry. It was used to verify the contributions by the anomalies and show what the thrust noise would have been without them. These results suggest that the CMNT with their existing performance model and control algorithm are capable of thrust noise levels that are more than 10x lower than the noise requirement for LPF. This model simulation can now be used to consider improvements to the controller to reduce noise further as necessary for the LISA mission or others.

ACKNOWLEDGMENTS

The research described in this paper was carried out by the Jet Propulsion Laboratory, California Institute of Technology, Goddard Space Flight Center and Busek Co. under contract with the National Aeronautics and Space Administration with our partners in this mission at ESA and on the LPF team. ESA support for the ST7-DRS mission elements and experiments was extraordinary. The authors would also like to thank NASA for support for the ST7-DRS mission.

REFERENCES

1. McNamara, P., et al., "LISA Pathfinder," *Classical Quantum Gravity*, 25, 114034 (2008).
2. Armano, M., et al. "Sub-Femto-g Free Fall for Space-Based Gravitational Wave Observatories: LISA Pathfinder Results," *Physical Review Letters* 116 231101 (2016).
3. Ziemer, J.K., Randolph, T.M., Franklin, G.W., Hruby, V., Spence, D., Demmons, N., Roy, T., Ehrbar, E., Zwalen, J., Martin, R., Connolly, W., "Delivery of Colloid Micro-Newton Thrusters for the Space Technology 7 Mission," AIAA- 2008-4826, 44th AIAA/ASME/SAE/ASEE Joint Propulsion Conference & Exhibit, 21-23 July 2008, Hartford, CT.
4. Ziemer, J., et al., "Colloid Microthruster Flight Performance Results from Space Technology 7 Disturbance Reduction System," IEPC 578-2017, 35th International Electric Propulsion Conference, 8-12 October, 2017, Atlanta, GA.
5. Hsu, O. C.et. al., "Dynamic Control System Performance During Commissioning of the Space Technology 7 – Disturbance Reduction System Experiment on LISA Pathfinder," AAS 17-155, Proceedings of the AAS GN&C Conference, Breckenridge, CO, February 2.
6. Maghami, P. G., O'Donnell, J. R. Hsu, O. H., Ziemer, J. K. , Dunn, C. E. "Drag-Free Performance of the ST7 Disturbance Reduction System Flight Experiment on the LISA Pathfinder," GNC 2017: 10th International ESA Conference on Guidance, Navigation and Control Systems, 29 May-2 June 2017, Salzburg, Austria.
7. O'Donnell, Jr., J. R. Hsu, O., Maghami, P., "Dynamic Control System Mode Performance of the Space Technology-7 Disturbance Reduction System," 68th International Astronautical Congress, 25–29 September 2017, Adelaide, Australia.

8. Hruby, V., Spence, D., Demmons, N., Roy, T., Ehrbar, E., Zwalen, J., Martin, R., Ziemer, J., Randolph, T., Connolly, W., Rhodes, S., Tolman, W., "ST7-DRS Colloid Thruster System Development and Performance Summary," AIAA-2008-4824, 44th AIAA/ASME/SAE/ASEE Joint Propulsion Conference, Hartford, CT, July 2008.
9. V. Hruby, et al, "Neutralizers for Electric Micro-propulsion Thrusters," 44th AIAA Joint Propulsion Conference, Hartford, CT, July 2008.
10. V. Hruby, et al, "Busek Colloid Thruster Development," *3rd Colloid Thruster Nano-Electrojet Workshop*, MIT, Boston, MA, April 14-15, 2005
11. Ziemer, J., "Performance of Electro spray Thrusters," IEPC-2009-242, 31st International Electric Propulsion Conference, Ann Arbor, MI, September 20-24, 2009.
12. J. Ziemer, et al., "Flight Hardware Development of Colloid Microthruster Technology for the Space Technology 7 and LISA Missions," 30th International Electric Propulsion Conference, IEPC-2007-288, Florence, Italy, September 2007.
13. N. Demmons, et. al., "ST7-DRS Mission Colloid Thruster Development," 44th AIAA Joint Propulsion Conference, Hartford, CT, July 2008.
14. Gamero-Casano, M., Hruby, V., "Electrospray as a source of Nanoparticles for Efficient Colloid Thrusters," *Journal of Propulsion and Power*, Vol. 17. No. 5, Sept-Oct. 2001.